Open Cavity Cooling Lattice for the Muon Collider

Pavel Snopok[*], Gail Hanson[†]
University of California, Riverside, CA 92521

Abstract

The RFOFO ring and its derivative Guggenheim helix are the two efficient lattices for the initial stage of cooling in the Muon Collider. However, they have a certain disadvantage, namely, the RF cavities operate in a strong magnetic field. R&D results to date suggest that this may cause breakdown of cavities before reaching desired RF gradients. The open cavity lattice studied in detail in this article attempts to address this problem by moving the magnetic coils into the irises of the RF cavities and shaping the cavities in such a way that the magnetic field lines are parallel to the walls. In such a layout the electrons do not gain enough energy to damage the walls, thus allowing the design gradients to be reached.

1 RFOFO cooling ring and Guggenheim helix

The RFOFO cooling ring and its derivative Guggenheim helix have been studied in detail in [1, 2, 3]. The layout of the RFOFO ring is shown in Fig. 1. A set of tilted magnetic coils generates transverse focusing and bending, while the RF cavities compensate for energy loss in the absorbers and provide longitudinal focusing. The Guggenheim helix is essentially the same RFOFO ring turned into a helix to provide for injection and extraction. In [3] it was shown that the RFOFO ring and the Guggenheim helix demonstrate similar performance: the six-dimensional emittance of the muon beam is reduced 448 times for an idealized RFOFO (360 times for Guggenheim), or 60 times for the realistic case with all the safety windows in the RF cavities and absorbers, in 495 meters of the cooling channel (15 turns). The parameters of the structures and performance graphs are summarized in the next sections, where they are compared to the parameters and performance of the open cavity layout [4, 5].

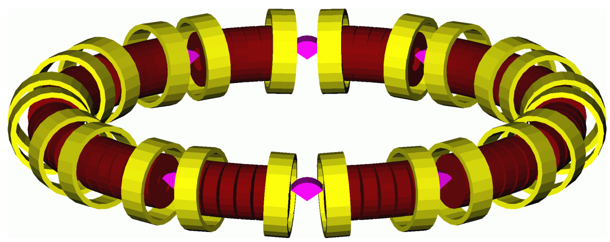

Figure 1: The RFOFO ring layout. Yellow—tilted magnetic coils with alternating currents to provide necessary bending and focusing and generate dispersion, magenta—wedge absorbers for cooling and emittance exchange, red—RF cavities for restoring the longitudinal component of the momentum.

2 Open cavity lattice parameters

The open cavity lattice uses the ideas of the original RFOFO ring; however, there are two essential differences:

- The magnetic coils are in the irises of the RF cavities, rather than outside and over the cavities.
- The RF cavity walls are shaped such that they

[*]snopok@gmail.com
[†]gail.hanson@ucr.edu

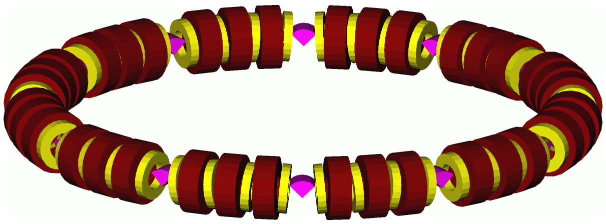

Figure 2: Open cavity ring layout. Yellow—tilted magnetic coils provide necessary bending and focusing and generate dispersion, magenta—wedge absorbers for cooling and emittance exchange, red—RF cavities for restoring the longitudinal component of the momentum.

> are aligned with the magnetic field in the region subject to developing breakdown. It is speculated [6], that in this case the electrons emitted from the surface of the wall will return to the surface with low energies and do no damage. However, for the purposes of the simulations presented in this paper the RF cavities are simulated as simple pillbox cavities.

The layout of the ring is shown in Fig. 2.

Table 1 summarizes the parameters of the open cavity lattice and compares them to the corresponding parameters of the RFOFO ring.

The RF gradient for the open cavity lattice is higher to compensate for the fact that the total length of RF per cell is shorter. For the same reason the absorber angle is smaller for the open cavity lattice as compared to the RFOFO ring. However, the open cavity design is more compact, yet the performance is similar, even somewhat better than of the RFOFO.

3 Magnetic field profiles

The ring layout consists of 12 identical cells. The magnetic field that focuses and bends particles and also provides the dispersion at the absorber is generated by four coils in each cell bearing currents with the following densities: 63 A/mm^2, 45 A/mm^2, -45 A/mm^2, -63 A/mm^2.

The profile of the magnetic field is more complicated for the open cavity ring, due to the fact that there are now four coils per cell as opposed to two in the RFOFO ring. However, the maximum magnetic field on axis is similar to the RFOFO ring—around 3 T. The radial component is larger than in the RFOFO ring, yet the order of magnitude is the same. The integrated on-axis radial field (hence, vertical beam deviations) is minimized by displacing the centers of the solenoids radially outward from the reference circle by 21 mm.

The fact that the solenoids are tilted leads to the reduction of the amount of space available for the RF system; hence, the energy gain per cell is limited, which, in turn, limits the angle of the wedge absorber to approximately 90° (*cf.* 110° in the RFOFO).

Figure 3 illustrates the difference between individual field components of the original RFOFO design and the new design with coils in the irises.

4 Closed orbits and dispersion

Because of the symmetry of the magnetic field, radial and vertical deviations of the closed orbit must be even functions of s at any energy. This requires that their derivatives must be zero at the ends of the period. Hence, closed orbits for different momenta can be found by scanning the plane $(x-y)$.

Deviations of the closed orbit along one periodic cell for various momenta ranging from 150 MeV/c to 250 MeV/c are shown in Fig. 4.

The dispersion calculation (Fig. 5) shows that the dispersion at the absorber plane (beginning of the cell) is primarily in the vertical direction, at an angle of ∼20° from the vertical axis. This fact suggests the orientation of the absorbers. The dispersion in the the center of the cell is negative, again mainly in the vertical direction.

5 Six-dimensional dynamics studies

The six-dimensional dynamics studies can be logically divided into two parts: with decay and stochastic processes off to observe cooling and estimate its

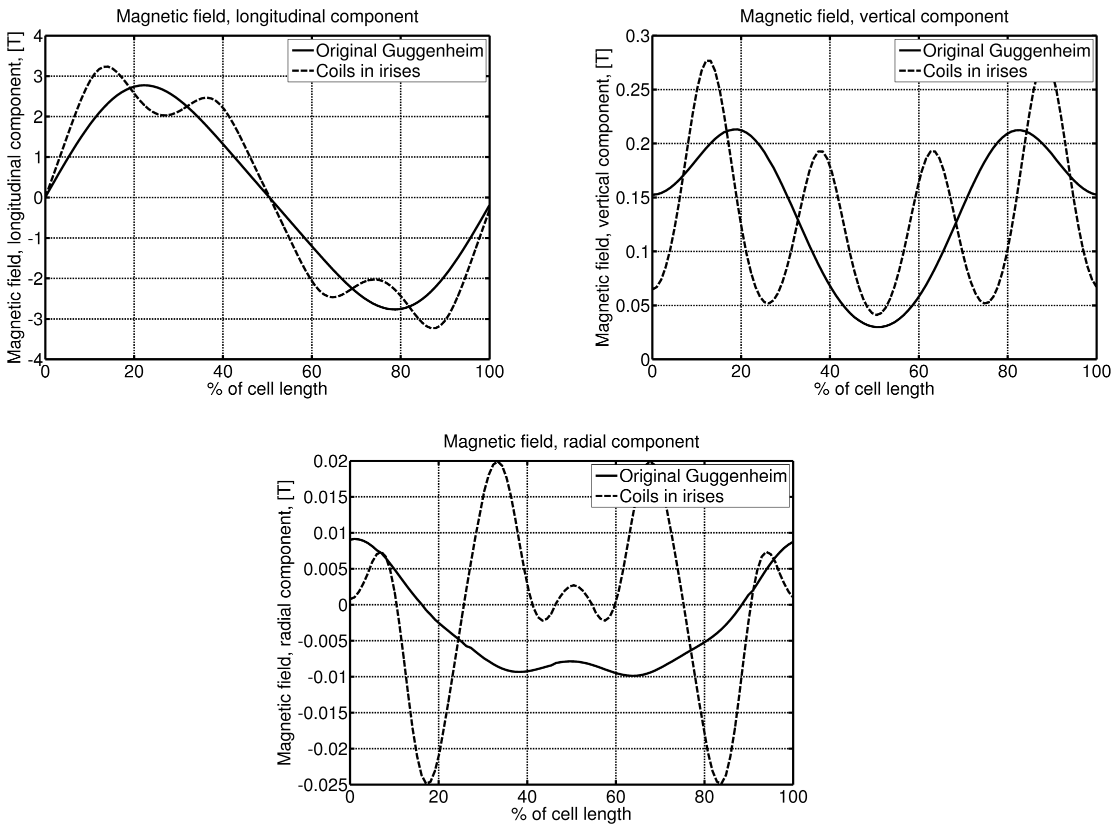

Figure 3: Longitudinal, vertical and radial components of the magnetic field. Solid line—original RFOFO ring (or Guggenheim helix), dashed line—open cavity lattice.

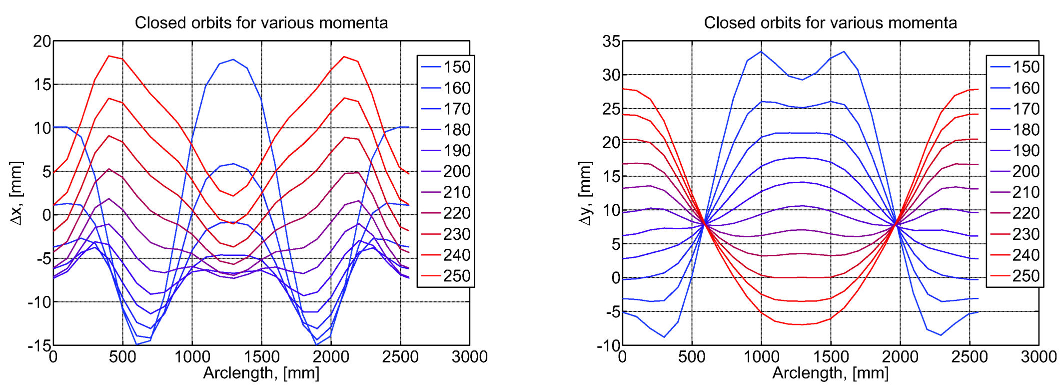

Figure 4: Closed orbit horizontal and vertical offsets along one cell of the cooling channel (2560 mm) for various momenta from 150 MeV/c to 250 MeV/c.

Parameter	Unit	Open cavity	RFOFO
Number of cells		12	12
Circumference	[m]	30.72	33.00
Radius	[m]	4.889	5.252
RF frequency	[MHz]	201.25	201.25
RF gradient	[MV/m]	16.075	12.835
Maximum axial field	[T]	3.23	2.80
Reference momentum	[MeV/c]	214	201
Coil tilt	[deg]	4.90	3.04
Number of coils per cell		4	2
Current densities	[A/mm^2]	$[63, 45, -45, -63]$	$[95, -95]$
Number of RF cavities		3	6
Length of each RF cavity	[mm]	385	282.5
Absorber angle	[deg]	90	110
Absorber vertical offset	[cm]	12.0	9.5
Absorber axial length	[cm]	24.00	27.13

Table 1: Parameters of the open cavity lattice compared to the RFOFO ring lattice.

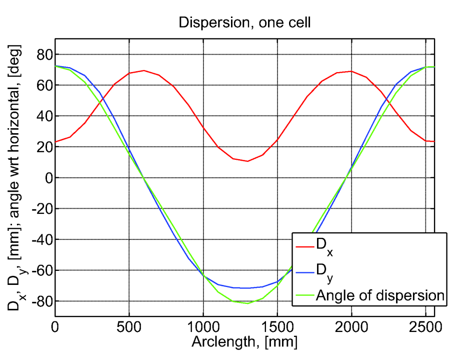

Figure 5: Dispersion plot for the reference particle. Red line—horizontal, blue line—vertical, green—orientation of dispersion with respect to the horizontal axis.

rate, as well as the rate of particle loss attributed to the structure, but not the muon decay.

The second part is to turn on the decay to see how it affects the transmission, and to turn on the stochastic processes to see how adding the heating term affects cooling efficiency.

The beam used for simulations has the following parameters:

- $\sigma_x = \sigma_y = 42$ mm;
- $\sigma_{p_x} = \sigma_{p_y} = 30$ MeV/c;
- $\sigma_t = 0.3$ ns;
- $\sigma_p = 26$ MeV/c;
- $\varepsilon_N^{\parallel} = 19$ mm;
- $\varepsilon_N^{\perp} = 12$ mm.

Certain correlations were introduced following [7] to account for linear dispersion and dependence of the revolution frequency on transverse momentum.

Tracking results for both approaches are illustrated and compared in Fig. 6. Observations:

- When the decay is off, after two turns the transmission becomes stable at 81%. The particles

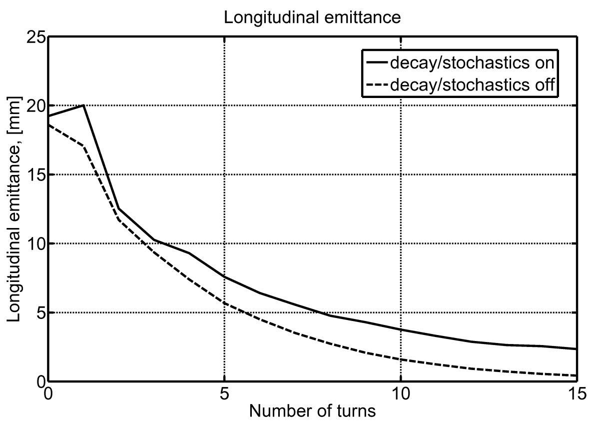

(a) longitudinal emittance

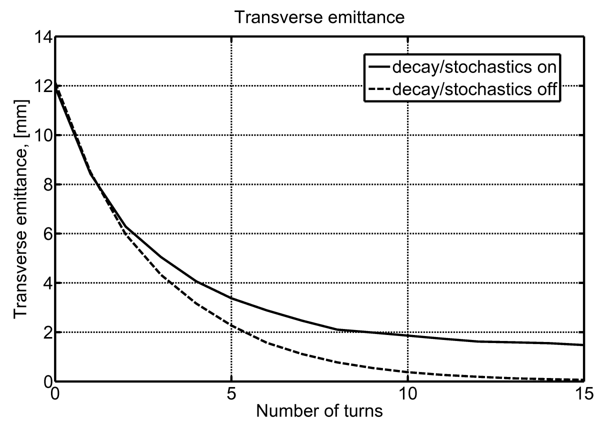

(b) transverse emittance

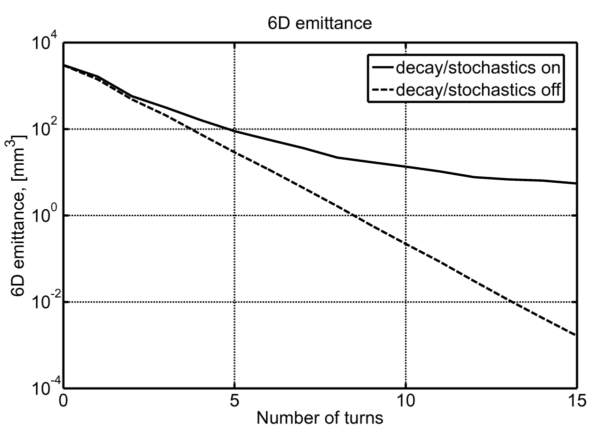

(c) six-dimensional emittance

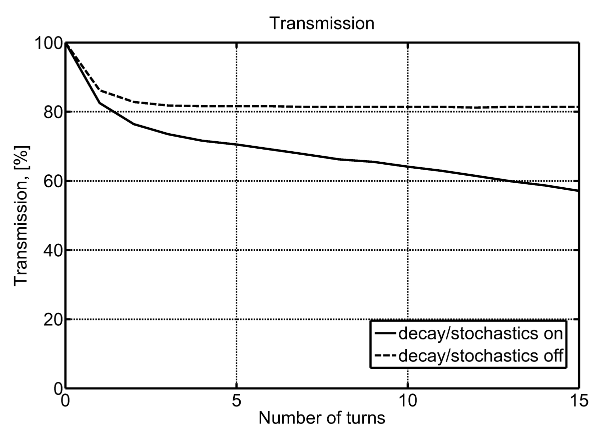

(d) transmission

Figure 6: Performance of the open cavity lattice with and without decay and stochastic processes. Solid line—decay and stochastic processes on, dashed line—decay and stochastic processes off.

which are lost either have large initial transverse amplitudes or are not captured in the stable RF bucket.

- Once the decay is on, after two turns the transmission is a linear function with a negative slope, all the loss is attributed to the decay.
- When the stochastic processes are off, there is no equilibrium emittance, hence, the six-dimensional emittance tends to zero, the rate of reduction is exponential (straight dashed line on the logarithmic plot).
- Once the stochastic processes are on, there is an equilibrium emittance (solid lines on the graphs), hence the six-dimensional emittance reduction is limited. In 15 turns (460.8 m) the six-dimensional emittance goes froom 3000 mm^3 to 5.5 mm^3.

The phase portraits of the beam after different number of turns with decay and stochastic processes off and on are shown in Fig. 7 and Fig. 8, respectively.

6 RFOFO and open cavity lattices compared

To draw conclusions about the cooling performance of the new open cavity lattice, it is important to compare the reduction in the longitudinal, transverse and six-dimensional emittance as well as the particle loss for the same initial conditions in both structures. These characteristics of both channels are compared in Fig. 9. The two structures are compared turn-wise; however, the circumference of the open cavity ring is 30.72 m, while the circumference of the RFOFO ring is 33.00 m. Hence, length-wise 15 turns in the open cavity lattice are almost the same as 14 turns in the RFOFO lattice. To take this fact into account, the performance characteristics of the RFOFO ring after 14 and 15 turns and of the open cavity ring after 15 turns are summarized in Table 2. Clearly, the performance of the open cavity lattice after 15 turns is better than that of the RFOFO after both 14 and 15 turns.

References

[1] R. Palmer et al., *Phys. Rev. ST Accel. Beams* **8**, 061003, 2005.

[2] A. Klier and G. G. Hanson, *Nuclear Physics B – Proceedings Supplements* **155, 1**, 277–278, 2006, DOI:10.1016/j.nuclphysbps.2006.02.072.

[3] P. Snopok, G. Hanson and A. Klier, *IJMPA* **24(5)**, 987–998, 2009.

[4] R. B. Palmer, J. S. Berg and R. Fernow, Open cell lattices, NFMCC Friday Meeting, March 23, 2007.

[5] R. Palmer et al., Cooling with magnetic insulation. Presentation at the 2009 NFMCC collaboration meeting, January 9, 2009, http://www.cap.bnl.gov/mumu/conf/MC-090125/talks/RPalmer1-090125.pdf.

[6] R. Palmer et al., RF breakdown with and without external magnetic fields, Tech. Rep. NFMCC-doc-528-v2, NFMCC, 2008.

[7] V. Balbekov, Simulation of RFOFO ring cooler with tilted solenoids, MUC-NOTE-THEORY-264, 2002.

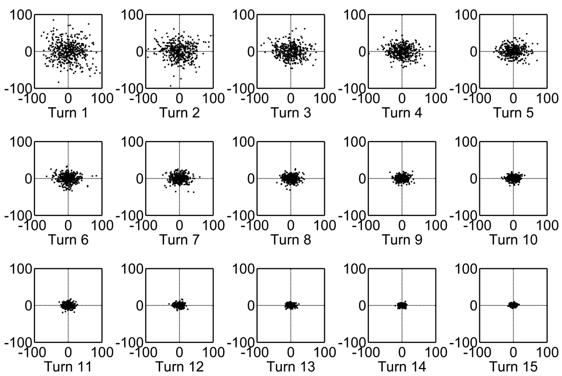

(a) $(x - p_x)$ plane

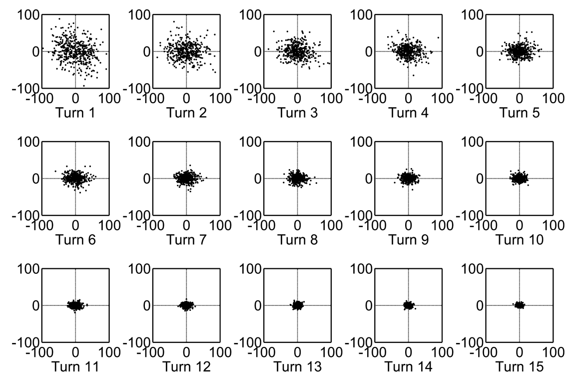

(b) $(y - p_y)$ plane

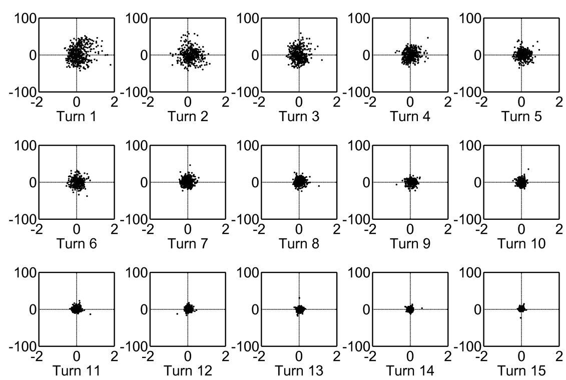

(c) $(t - p_z)$ plane

Figure 7: Phase portraits in the $(x - p_x)$, $(y - p_y)$ and $(t - p_z)$ planes, decay and stochastic processes off. No equilibrium emittance, the beam emittance goes to zero exponentially.

Parameter	Unit	Initial	Open cavity 15 turns	RFOFO 14 turns	RFOFO 15 turns
$\varepsilon_\perp$	[mm]	12	1.5	1.7	1.6
$\varepsilon_\parallel$	[mm]	19	2.3	2.5	2.4
ε_{6D}	[mm^3]	3000	5.5	7.2	6.7
Transmission	[%]	100	57	56	54

Table 2: Parameters of the open cavity lattice compared to the RFOFO ring lattice.

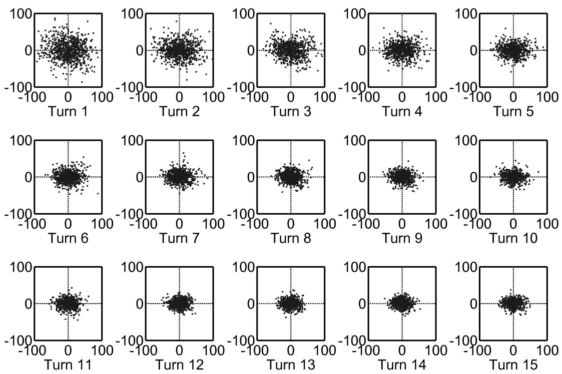

(a) $(x - p_x)$ plane

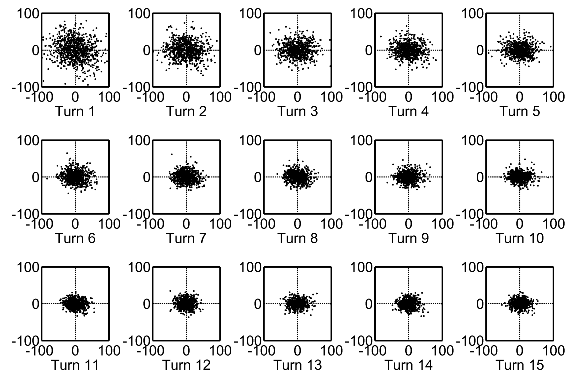

(b) $(y - p_y)$ plane

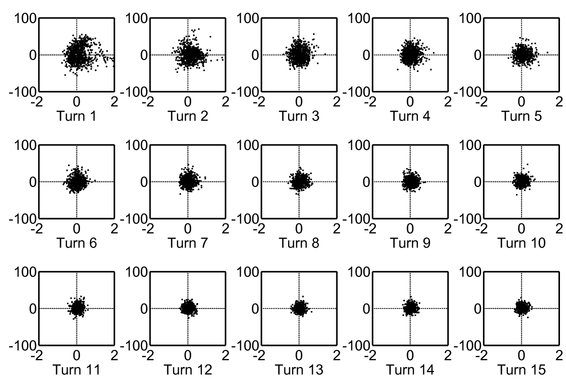

(c) $(t - p_z)$ plane

Figure 8: Phase portraits in the $(x - p_x)$, $(y - p_y)$ and $(t - p_z)$ planes, decay and stochastic processes on. The beam emittance is reduced until the equivilibrium emittance is reached.

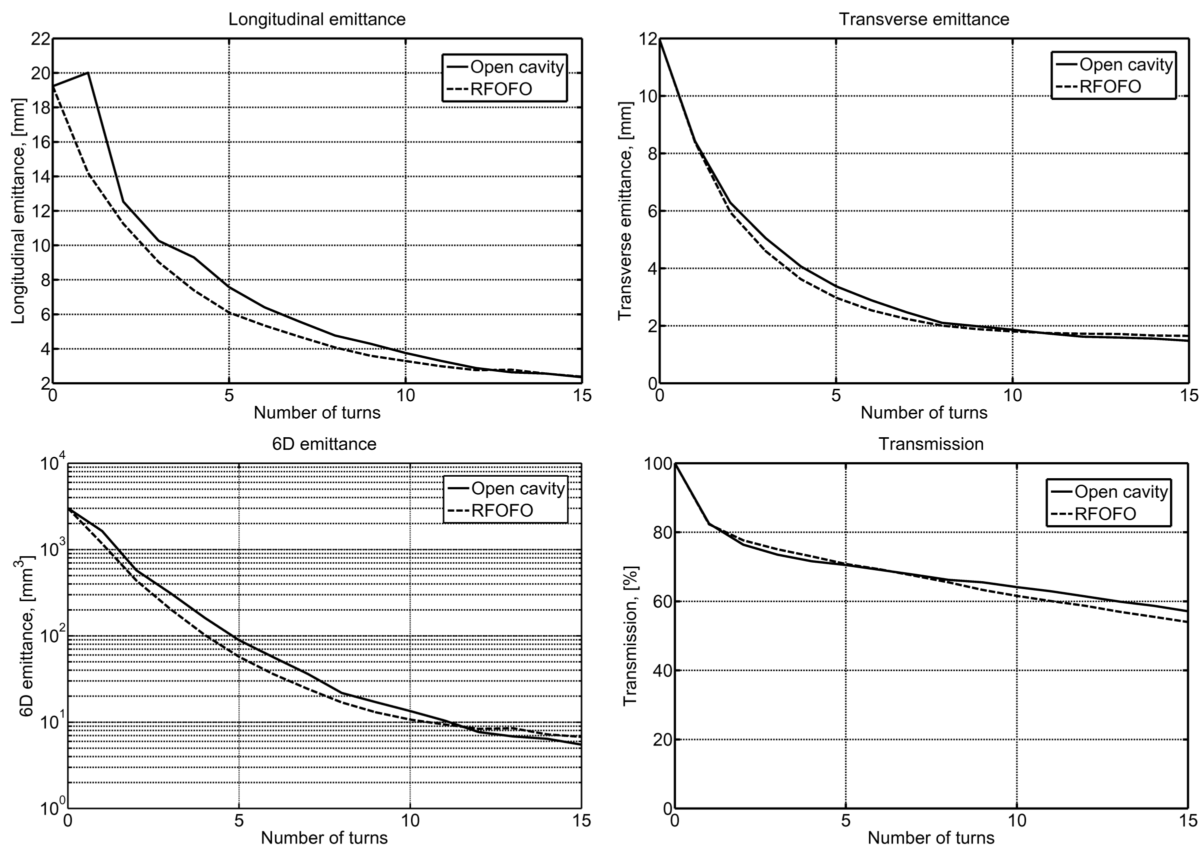

Figure 9: Performance of the open cavity lattice *vs.* the RFOFO lattice with decay and stochastic processes. Solid line—open cavity lattice, dashed line—RFOFO lattice.